Journal of Solid State Chemistry 182 (2009) 2733–2742

Contents lists available at ScienceDirect

Journal of Solid State Chemistry

journal homepage: www.elsevier.com/locate/jssc

Photochemical modification of magnetic properties in organic low-dimensional conductors

Toshio Naito [a,b,*], Akihiro Kakizaki [b], Makoto Wakeshima [b], Yukio Hinatsu [b], Tamotsu Inabe [b]

[a] Creative Research Initiative Sousei (CRIS), Hokkaido University, Sapporo, Hokkaido 001-0021, Japan
[b] Division of Chemistry, Graduate School of Science, Hokkaido University, Kita 10, Nishi 8, Kita-ku, Sapporo, Hokkaido 060-0810, Japan

ARTICLE INFO

Article history:
Received 14 May 2009
Received in revised form
14 July 2009
Accepted 18 July 2009
Available online 25 July 2009

Keywords:
Organic charge transfer salt
Low-dimensional conductor/magnet
Photochemical reaction
Conducting/magnetic property

ABSTRACT

Magnetic properties of organic charge transfer salts Ag(DX)$_2$ (DX = 2,5-dihalogeno-*N*,*N*′-dicyanoquinonediimine; X = Cl, Br, I) were modified by UV irradiation from paramagnetism to diamagnetism in an irreversible way. The temperature dependence of susceptibility revealed that such change in magnetic behavior could be continuously controlled by the duration of irradiation. The observation with scanning electron microprobe revealed that the original appearance of samples, e.g. black well-defined needle-shaped shiny single crystals, remained after irradiation irrespective of the irradiation conditions and the duration. Thermochemical analysis and X-ray diffraction study demonstrated that the change in the physical properties were due to (partial) decomposition of Ag(DX)$_2$ to AgX, which was incorporated in the original Ag(DX)$_2$ lattices. Because the physical properties of low-dimensional organic conductors are very sensitive to lattice defects, even a small amount of AgX could effectively modify the electronic properties of Ag(DX)$_2$ without making the original crystalline appearance collapse.

1. Introduction

More than 30 years, the organic charge transfer salts have been at the center of scientific and technological interest in the field of synthetic (semi) conductors [1–3]. Their building blocks are generally planar molecular radical species with low symmetries and extended π-conjugations (Fig. 1), and their electronic band structures depend on π–π overlaps between neighboring molecules (Fig. 2). The anisotropy of the π-orbitals commonly leads to highly anisotropic (i.e. low-dimensional) crystal structures as well as small band widths (∼1/2–1/10 of those of other kinds of conductors). For example, they consist of nanowires (one-dimensional, 1D), nanosheets (two-dimensional, 2D), and so on, all of which are made of molecular networks based on π–π interactions. Such characteristic molecular arrangements necessarily lead to high anisotropy in physical properties as well. Roughly speaking, the lower the dimensionality becomes, the less the number of the nearest neighbor sites become. Therefore the lower dimensionality involves a smaller number of intermolecular interactions, which are basically weak van der Waals interactions, dominating electrical and magnetic properties. Accordingly these structural situations peculiar to molecular charge transfer salts make the resultant electronic system far more sensitive to perturbations such as structural change [1–3], magnetic field [4–11], and lattice defects [12] than usual conductors having isotropic structures. This is one of the reasons the organic charge transfer salts are interesting in terms of sensors and devices.

Although the organic conductors, especially in their single crystalline forms, have many unique electrical and magnetic properties stated above, which might be applied to novel device actions, a serious drawback against practical application is the difficulty in controlling the physical properties of a given material with sufficiently high spatial resolution. As such a method, doping has played an indispensable role in fabrication of the current silicon-based semiconductor devices. However, standard ways of doping are not always practical in crystalline organic charge transfer salts. Thermal instability and mechanical fragility prevent us from the application of most of the advanced fabrication techniques established in inorganic semiconductors industry. In addition, most organic charge transfer salts are insoluble in any solvent and not volatile without decomposition, which limits our methods to treat them. The only practical and versatile way is chemical mixing in the course of syntheses. However, inclusion of foreign chemical species in the crystals of organic charge transfer salts often results in serious lowering of the crystal qualities and thus deteriorating of the conducting/magnetic properties. Coexistence of foreign chemical species (dopants) in synthesis sometimes led to unexpected change in crystal structures and thus in

* Corresponding author at: Creative Research Initiative Sousei (CRIS), Hokkaido University, Sapporo, Hokkaido 001-0021, Japan. Fax: +81 11 706 3563.
E-mail address: tnaito@sci.hokudai.ac.jp (T. Naito).

0022-4596/$ - see front matter © 2009 Elsevier Inc. All rights reserved.
doi:10.1016/j.jssc.2009.07.032

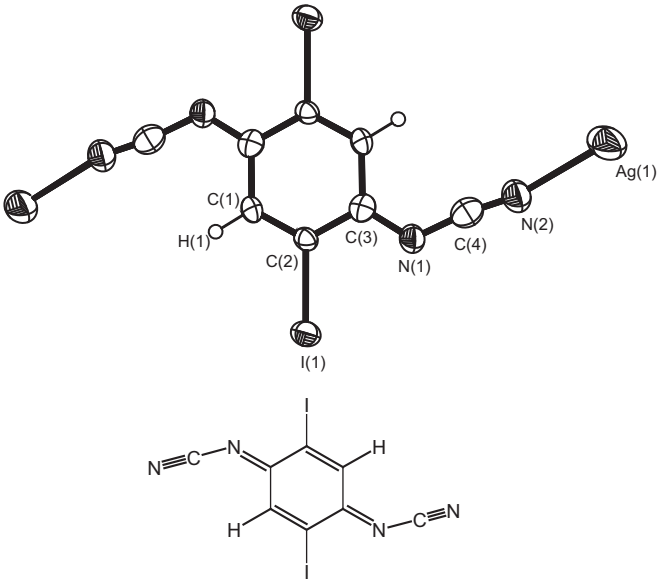

Fig. 1. Molecular structure of *DI* shown with silver ions coordinated by the imino-groups (=N–CN) of *DI*.

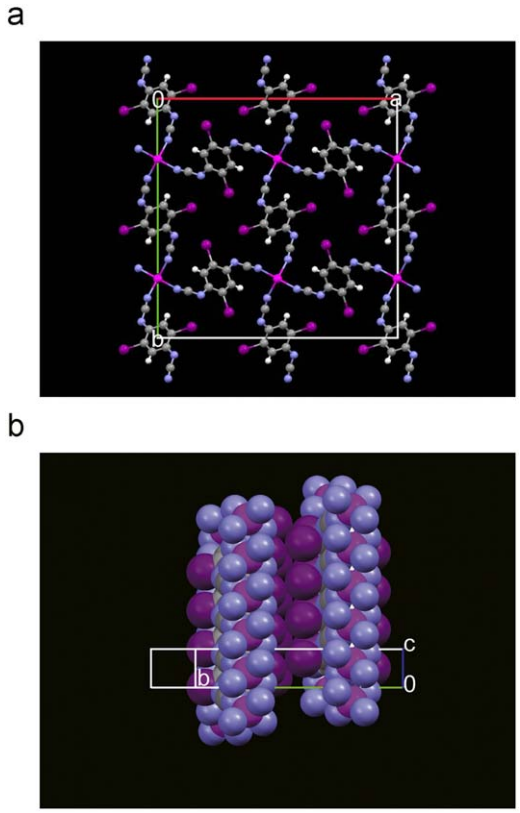

Fig. 2. Crystal structure of $Ag(DI)_2$; (a) view down along the *c* axis (stacking axis), and (b) perpendicular to the *c* axis. Purple, dark violet, grey, white, and pale blue spheres designate Ag, I, C, H, and N atoms, respectively.

physical properties [13,14]. It is very difficult to control exact amount of dopant and the precise part to be doped by chemical mixing methods.

A solution to these difficult problems was proposed in 2004; a photochemical method to control the number of carriers (unpaired electrons) with spatial resolution [15–21]. Utilizing this method a single crystal of $Ag(DM)_2$ (DM = 2,5-dimethyl-*N*,*N*′-dicyanoquinonediimine) can be irreversibly transformed to a diode, which have a junction interface between the irradiated and the non-irradiated parts in the crystal. Once the irradiation ceases, the resultant material are stable to retain the modified conductivity under normal atmosphere, or one can resume the irradiation to further modify the electrical property. The absolute values and temperature-dependence of resistivity gradually and continuously varied from metallic to semiconducting ones in accordance with temperature-controlled irradiation with UV and/or Visible (Vis) light. Meantime the magnetic properties varied from Pauli paramagnetic to Curie-like behavior, which was consistent with the change in electrical behavior mentioned above. Although such modification in magnetic property is of a qualitative level (from that of a metal to that of a semiconductor), both properties are paramagnetic, and thus a more marked change is desirable for future practical application in memory devices; for example, transformation between magnetic and non-magnetic properties. Here we report such materials, which alter their paramagnetism to diamagnetism simply by UV irradiation only in regard to the irradiated parts.

2. Experimental section

2.1. Synthesis

The chemicals were purchased from Sigma-Aldrich, Inc. or Wako Pure Chemical Industries, Ltd. in their purest grades and used as received. Silver wires (1 mm ∅, 99.99%) were purchased from The Nilaco Corporation and used in the synthesis of the silver salts. 2,5-dihalogeno-*N*,*N*′-dicyanoquinonediimine (*DX*; Fig. 1) were prepared according to the literature [22,23]. Their silver salts $Ag(DX)_2$ in single crystals were prepared with a slight modification of a reported procedure [22,23]. In our typical procedure, *DX* (X = Cl: 100 mg, Br: 60 mg, I: 10 mg) and $AgNO_3$ (X = Cl, Br: 2 mg, I: 1 mg) were dissolved in CH_3CN (X = Cl, Br: 60 mL, I: 40 mL) and the solution was sealed, stood still for 30 min at −30 °C. Then a silver wire freshly cut in length of 5 mm was added in the solution, and the solution was again sealed, kept at −30 °C for 7–10 days to yield black thick needles of $Ag(DX)_2$. Thus obtained single crystals were analytically pure and many of them were suitable for structural analyses and physical property measurements.

2.2. UV-irradiation

For irradiation of the samples, one of the following UV light sources ((A), (B) and (C)) was used; (A) a Hg/Xe-lamp (200 W; Hamamatsu Photonics K. K.; Supercure-203S UV Lightsource; San-Ei Electric) with a multimode quartz fiber (1 m—length, ϕ = 5 mm, numerical aperture (NA) = 0.22), (B) a Xe-lamp (100 W; Asahi Spectra K. K.; LAX-Cute) with a multimode quartz fiber (1 m—length, ϕ = 5 mm, NA = 0.2), and (C) a UV laser (375 ± 5 nm, 20 mW, NEOARK TC20-3720-15) with a light guide (1 m—length) of adjustable focus, *NA*, and size of the beam spot. (A) was equipped with a filter and a mirror for filtering light with wavelengths of 220–275 nm. This helps to minimize thermal effects during the irradiation of the sample. (B) was equipped with a mirror module and a filter to irradiate the samples with the light of 240–360 nm wavelengths only. (B) was also equipped with a rod lens, which realizes a homogeneous irradiation with being in/out of focus to adjust the spot size to the sample area. The intensity of light at the sample was measured with a power meter (Ophir, NOVA attached with a Si photodiode head PD-300-UV).

The maximum power varied with the wavelength. At several wavelengths, the light was particularly intense due to the characteristic spectral lines of Hg and Xe. For example, the intensity was 20 mW/cm^{-2} at 275 nm for (A), and 17 mW/cm^{-2} at 240 nm for (B). As for the light source (C) typical conditions of the laser at the sample position are 14–17 mW/cm^{-2} and the beam spot $\phi = 3$–5 mm. When many single crystals are required to be homogeneously irradiated in equal conditions, the single crystals were irradiated while they were suspended and stirred in water. This method enabled us easy control of temperature and homogeneous irradiation of the samples. After irradiation in water, the samples were examined with spectroscopic methods, scanning electron microprobe (SEM), and elemental analysis, and were found to have no difference in the spectroscopic and analytical results compared with those irradiated in air or vacuum. Ozone is known to evolve under UV irradiation in air with wavelengths shorter than 220 nm, which were not used in our experiments. The following experiments could not be carried out on a single crystal; X-ray photoelectron spectra (XPS), magnetic susceptibility, differential scanning calorimetry (DSC), thermogravimetric and differential thermal analysis (TG-DTA), IR and mass (MS) spectroscopies, and powder X-ray diffraction (XRD) measurements. Thus the single crystals were ground to a fine powder (agate mortar and pestle) and exposed to UV light. After grinding, the powder samples were examined with spectroscopic methods, SEM, XRD and elemental analysis, and were found to have no difference in the spectroscopic and analytical results compared with those before grinding. In water, air, or vacuum ($\sim 5 \times 10^{-7}$ Pa), irradiation provided the samples an approximately similar intensity of light, since air and water do not have strong absorption at $\geq$220 nm. The sample temperature during irradiation was monitored with a Si-diode sensor (Lakeshore DT-470) by setting it immediately beside the sample.

2.3. Characterization methods

XRD patterns were measured at room temperature (RT) with either X-ray diffractometer of a Rigaku R-INT 2000 or a Rigaku RINT-Ultima+. The Rigaku RINT-UltimaIII was also used to examine the relationship between thermodynamic changes (DSC) and structural changes (XRD) from RT-500 °C. X-ray study (data collection) for crystal structural analyses on Ag(DX)$_2$ was carried out with a Rigaku R-AXIS RAPID-S Imaging Plate area detector with graphite monochromated Mo$K\alpha$ radiation ($\lambda = 0.7107$ Å) at 23 ± 1 °C. The intensities were corrected for Lorentz and polarization effects. Empirical absorption correction was applied. Structures were solved by direct methods (SHELX97) [25], and refined by full-matrix least-squares on F^2 using all the independent reflections obtained. Anisotropic thermal parameters for non-hydrogen atoms and isotropic ones for hydrogen atoms (thermal parameters are 1.2 times those of the attached carbons) were employed for the structure refinement. The function minimized was $\sum w(F_o^2 - F_c^2)^2$, where w means least square weights $1/[1.0000\sigma(F_o^2)]/(4F_o^2)$. Hydrogen atoms were placed at the calculated ideal positions, and were included but not refined. Atom scattering factors were taken from the literature [26]. The values for the mass attenuation coefficients are those of Creagh and Hubbell [27]. All calculations and a part of the molecular graphics were performed using the crystallographic software package "CrystalStructure" [28] and some structural views were produced using Ortep3 for Windows [30]. DSC and TG-DTA experiments were carried out using a Rigaku Thermo Plus2 DSC8230 and a Rigaku Thermo Plus TG 8120 TG-DTA, respectively. Platinum pans were used for both DSC (except for XRD–DSC) and TG-DTA, while aluminum pans were used in XRD–DSC. The temperature dependence of the magnetic susceptibility was measured on polycrystalline samples using a superconducting quantum interference device (SQUID) (MPMS-5S and MPMS-5X, Quantum Design). The applied fields were 0.8–1 T. Different sequences (heating/cooling processes) are examined on different/the same samples using different machines in order to check any artefact or metastable state. The diamagnetic susceptibilities of neutral DX molecules were measured ($-\chi_{dia}^{DX} \times 10^5$ cm^3/mol = 6.296 (X = Cl), 6.504 (X = Br) and 9.957 (X = I), respectively), while that of the Ag^+ ions (-3.10×10^{-5} cm^3/mol) was taken from a literature [31]. Using a home-made cryostat, the electrical resistivity was measured with a standard four-probe method along the longitudinal direction of needle-shaped single crystals. This direction coincides with the crystallographic c axis, which is most conductive direction in Ag(DX)$_2$. Gold wires (25 μm in diameter) and gold paste (No. 8560, Tokuriki Chemical Research Co., Ltd.) were used as electrical contacts. For checking reproducibility and sample dependences, the magnetic susceptibility and resistivity measurements were repeatedly (5–10 times) examined using the same samples as well as different samples independently prepared/irradiated. Matrix-assisted laser desorption ionization (MALDI) time-of-flight mass spectra were measured by Voyager-DE STR-H (Applied Biosystems). Standard matrix compounds such as 2,5-dihydroxybenzoic acid ($(HO)_2C_6H_3CO_2H$ = 154.12) and α-cyano-4-hydroxycinnamic acid ($HOC_6H_4CH{=}C(CN)CO_2H$ = 189.17) were used as calibration matrix. However, the simplest spectra were obtained when no matrix was used in the sampling; otherwise, most of the standard matrix compounds reacted with the original and/or the fragment species to give complicated spectra with poor reproducibility. Both positive and negative charged species were detected under various measurement conditions. A typical condition was as follows; extraction delay time = 110 ns, acquisition mass range = 100–2500 u, number of laser shots = 1000/spectrum, laser repetition rate = 3.0 Hz. A JEOL JSM-6360LA scanning electron microprobe was used for observation of the single crystals before and after irradiation. XPS were measured using JPS-9200 (JEOL) on pressed powder pellets (~0.5–0.8 mm thick, 5–10 mm in diameter) of pristine and irradiated Ag(DX)$_2$. The spatial and energy resolutions of this equipment are ~30 μm and ~1 eV, respectively. The samples were directly set on the sample stage made of titanium (Ti-stage) without any kind of glue or tapes so that one could measure the XPS of the bottom surface after the measurement of the upper surface. The samples were earthed through the Ti-stage and supposed to be free from charge-up effects. In order to check if each sample was actually free of a charge-up effect, another sample was set on a Ti-stage with a conductive carbon tape for SEM (Nisshin EM) or using a minimum amount of conductive gold paste (No. 8560, Tokuriki Chemical Research Co., Ltd.) for comparative check of the spectra. In these cases the carbon tapes/gold paste were completely covered with the samples so that photoelectrons from the tapes/paste should be negligible. Standard spectra (Ag 3d, Cl 2p) of AgCl (Wako, 99.5%) were measured by setting the powder on the carbon tapes attached on the Ti-stage. AgCl was not darkened after XPS measurements, and the standard spectra were reproducible. The obtained binding energies (BEs) did not depend on sample forms/settings. As preliminary measurements, every sample was exposed to electron beams of various energies (accelerating voltages of 0–20 V)/intensities (filament currents of 0–6 A) during XPS measurements, and we compared the obtained spectra to confirm that charge-up effects were negligible considering the energy resolution of this equipment (~1 eV). The binding energies were cross-checked using oxygen peaks. As for Ag(DCl)$_2$, firstly, the surface of the pristine sample were sputtered for a few minutes with Ar^+ beam in the XPS spectrometer ($\sim 5 \times 10^{-7}$ Pa),

and then irradiated with the light source (C) *in situ*. XPS were measured on the beginning and every 6–12 h during the UV irradiation (0, 1, 3, 6, 12, 24, 48, 53, 64, 72, 81 h, 4 and 7 days). Some pellets were partly irradiated in order to examine the spatial resolution of the irradiation effects. In the curve-fitting analyses of the obtained XPS, the validity of the deconvolution was checked by comparison of the resultant parameters (peak positions, splittings, (relative) intensities, linewidths) with those of similar compounds. Polarized reflectance spectra were measured on single crystalline samples at RT using an IR spectrometer FT/IR-6100 attached with a microscope IRT-3000 (JASCO). The polarization angles were parallel (||*c*-spectrum) or perpendicular (⊥*c*-spectrum) to the *c* axis (most conductive direction). The aperture (and thus the IR beam spot) was rectangular and could be rotated, and its longer and shorter sides were independently adjustable to the sample sizes and shapes. A typical size of the spot was $\sim 50 \times 150\,\mu m^2$ and the smallest size was $\sim 20 \times 30\,\mu m^2$, which was dependent on the signal to noise (S/N) ratio and technically determined the spatial resolution in this analysis ($\sim 30\,\mu m$). The polarizer was rotated by a step of 5°, being independent of the aperture setting. Mirror surfaces of several samples were selected to examine in order to check sample- and part-dependence and reproducibility. Evaporated gold film was used to give the standard reflection (100%) intensity at all the measured wavelengths. ESR was measured using an EMX EPR spectrometer (Bruker) at RT when the magnetism should be checked on a small amount of sample such as a single crystal. Microscopic observation of the single crystal irradiated for 3.5 h with the light source (A) was carried out using Nanoscale hybrid microscope VN-8000 (KEYENCE), which enabled us observation and 3D measurements of a particular point of the sample surface from sub-millimeter to nanometer ranges in a series of observation, i.e. without re-setting the sample.

3. Results and discussion

3.1. Crystal structures of pristine Ag(*DX*)$_2$

All Ag(*DX*)$_2$ (*X* = Cl, Br, I) are known to be isomorphous [22,23,32–42] from X-ray measurements of their lattice parameters, yet their full structural analyses (atomic parameters) have not been reported. Their unit cell is shown in Fig. 2 and structural summary is given in Table 1. When *DX* forms a salt with metallic silver in solution, a charge- (electron-) transfer occurs between the *DX* molecules and the Ag atoms. As a result a certain fraction of the *DX* molecules formally exists as a radical anion species, while the Ag atoms become monocations thus maintaining charge neutrality in the whole solid.

In the crystal the *DX* molecules stack to form a columnar structure. The unpaired electrons on the anion radical species delocalize along these columns, resulting in a highly anisotropic (1D) conduction. Cooperative phenomena such as electrical and magnetic properties are particularly sensitive to lattice defects in the 1D system.

Another unique feature of *DM* arises from the two =N–CN groups at both ends of the π-conjugation system of the molecule. They comprise the π-conjugation system and play a key role in stabilizing the radical anion state by delocalizing the unpaired electrons in the π-molecular orbital. At the same time, the =N–CN group, like the cyano group (–CN), is strongly coordinating and all the DM molecules are bonded with the Ag^+ ions through the =N–CN groups. The bond lengths (interatomic distances) of Ag–N are 2.308(2) (*X* = Cl), 2.298(2) (*X* = Br) and 2.310(7) Å (*X* = I). These coordination bonds form a 3D polymeric structure.

Table 1
Crystal data and structural analysis summary for Ag(*DX*)$_2$ (*X* = Cl, Br, I).

Compound	Ag(*D*Cl)$_2$	Ag(*D*Br)$_2$	Ag(*D*I)$_2$
Formula	$C_{16}H_4N_8Cl_4Ag$	$C_{16}H_4N_8Br_4Ag$	$C_{16}H_4N_8I_4Ag$
Formula weight	557.94	735.75	923.75
Crystal system	Tetragonal	Tetragonal	Tetragonal
Space group	$I4_1/a$	$I4_1/a$	$I4_1/a$
a (Å)	22.35(1)	22.39(1)	22.46(1)
c (Å)	3.765(2)	3.868(2)	4.074(2)
V (Å^3)	1881(1)	1939(2)	2056(2)
Z	4	4	4
D_x (g cm^{-3})	1.970	2.520	2.985
μ(MoKα) (cm^{-1})	16.586	93.278	70.100
$2\theta_{max}$ (deg)	55.0	54.9	55.0
Temp. of data collections (K)	296	296	296
No. of reflections	8314	8536	9054
No. of unique reflections	1072	1099	1180
R_{int}	0.099	0.033	0.071
No. of variables	67	67	67
R [$I > 2.0\ \sigma(I)$][a]	0.0296	0.0418	0.0420
R[b]	0.0538	0.0472	0.0530
R_w[b,c]	0.0861	0.1249	0.1089
Goodness of fit indicator	0.511	0.904	1.017

[a] $R = \Sigma\ ||F_o| - |F_c|| / \Sigma\ |F_o|$.
[b] For all reflections.
[c] $R_w = [\Sigma(\omega(F_o^2 - F_c^2)^2) / \Sigma\omega(F_o^2)^2]^{1/2}$.

3.2. Thermal properties of pristine Ag(*DX*)$_2$

As well as structural information, information on chemical and thermal stabilities is important in discussion on photochemical reactions and the resultant change in the physical properties of Ag(*DX*)$_2$. It is difficult to irradiate a sample completely without heating effects, while it is facile to heat the sample completely without light. Thermal analyses enable us to distinguish thermal processes from photochemical processes, i.e. inform us on what kind of changes are possible solely by heating the sample. The results of XRD–DSC on powder Ag(*D*Cl)$_2$ are shown in Fig. 3. The corresponding results on the other compounds Ag(*DX*)$_2$ (*X* = Br, I) are deposited as supplementary material (Figs. S1(a)–(f)). The results did not vary when the measurements were carried out in air or under nitrogen atmosphere, and did not depend on humidity in the sample room. In DSC the three salts exhibited similar behavior; exothermic peaks at ~140 (T_1) and ~380 °C (T_2) implying some change to a stabler state occurred at each temperature. Powder XRD results can be clearly divided in three patterns. Below the temperature of the exothermic peak T_1 ($\approx$142 (*X* = Cl), 141 (*X* = Br), and 149 °C (*X* = I)) the XRD patterns (A) retained the original features of those of Ag(*DX*)$_2$, which means that all the three salts retained their original crystalline structures below T_1. Above T_1 up to ~170 °C the diffraction peaks due to Ag(*DX*)$_2$ disappeared (B). In the meantime powder XRD patterns due to Ag*X* appeared and developed with temperature in all the three salts, which means progressive decomposition of Ag(*DX*)$_2$ into Ag*X* above T_1. Slightly above T_1, the powder XRD patterns of all the salts became featureless. This is because most of the crystalline lattices of Ag(*DX*)$_2$ were lost, while the amount of Ag*X* was too small to give obvious features in the powder patterns. Under UV–Vis irradiation, a related material Ag(*DM*)$_2$ (*DM* = 2,5-dimethyl-*N*,*N*′-dicyanoquinonediimine) completely became amorphous without melting or decomposition, perfectly retaining the original crystalline appearances except for the color [16–21]. Around 373 °C, which was near T_2 ($\approx$377 (*X* = Cl), 375 (*X* = Br), and 376 °C (*X* = I)), the XRD peaks due to Ag*X* disappeared and those due to the Al pans were exclusively observed (C). This indicates that no long-range order in the structure should be present in the sample. Melting points of Ag*X*

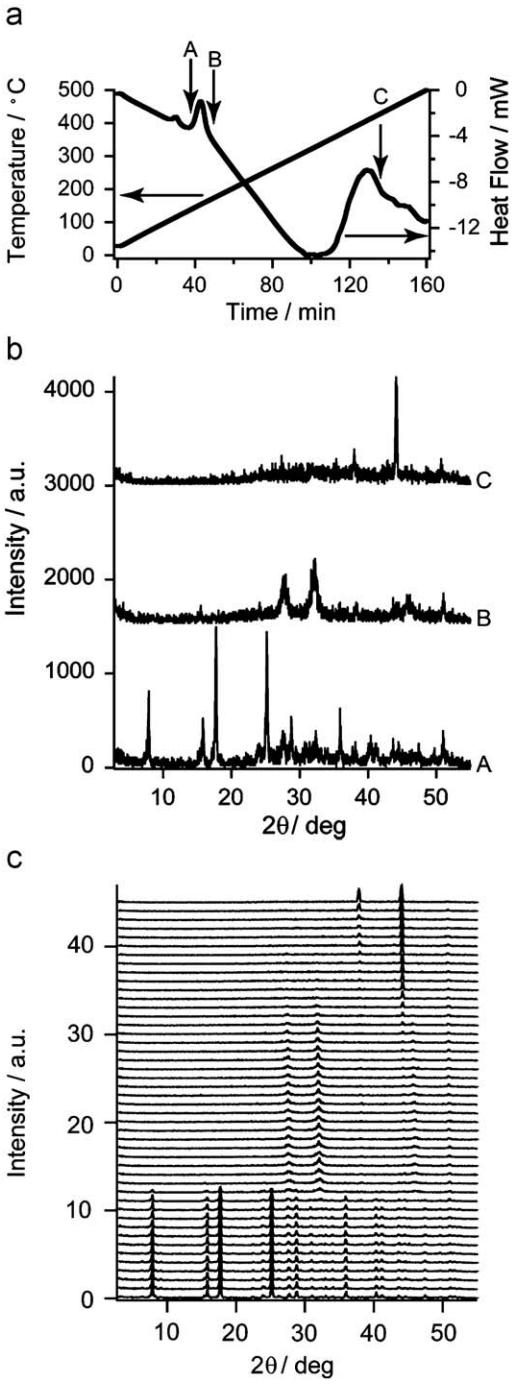

Fig. 3. XRD–DSC of Ag(*D*Cl)$_2$. DSC and powder X-ray diffraction patterns were simultaneously measured while the sample temperature was constantly and slowly raised from RT to 500 °C. Selected XRD patterns at temperatures of interest are shown in (b); each XRD patterns were measured in the following temperature ranges, A: 129.7–140.0, B: 160.8–170.7, C: 353.6–363.8 °C. All the observed XRD patterns in XRD–DSC are shown (measured at ~every 10 °C) in (c). In (c), the XRD patterns are arranged in a temperature-increasing order from RT (bottom) to 500 °C (top).

(AgCl 455 °C, AgBr 432 °C, AgI 552 °C) are well above these temperatures (T_2), and thus the anomalies at T_2 can be irrelevant to melting.

The results of TG-DTA on Ag(*D*I)$_2$ are shown in Fig. 4. The corresponding results on the other compounds Ag(*DX*)$_2$ (X = Cl, Br) are deposited as supplementary material (Figs. S2(a) and (b)). For exothermic peaks appeared at 150 and 376 °C, which agreed with the results of DSC (T_1 and T_2) in a quantitative way. Around

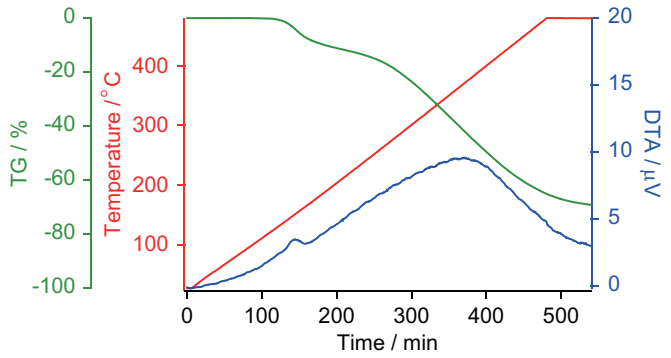

Fig. 4. TG-DTA of Ag(*D*I)$_2$.

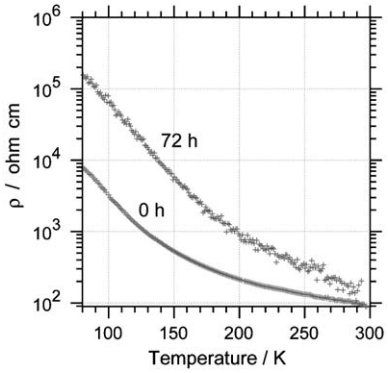

Fig. 5. UV irradiation effects in the electrical resistivity of Ag(*D*I)$_2$ measured along the *c* axis of the single crystals after continuous UV (240–360 nm) irradiation; temperature-dependence of pristine (0 h) and irradiated (72 h) samples. The sample temperature did not exceed 30 °C during irradiation.

170 °C, where Ag(*D*I)$_2$ should be structurally decomposed based on the XRD–DSC results above, the sample mass decreased only by ~5% of the original value. Such a decrease in the mass is too small to assume complete decomposition of Ag(*D*I)$_2$ to AgI. Ag(*DX*)$_2$ do not melt at ≤170 °C. Therefore Ag(*D*I)$_2$ around 170 °C should be a mixture of Ag(*D*I)$_2$ and AgI. Then, on increasing temperature further, more and more of the sample decomposed, and obvious decrease in the mass suddenly began around 400 °C until 60–80% of the original mass was lost by 500 °C. The total decrease in the mass corresponds to decomposition and loss of ~90% of *D*I molecules in the original Ag(*D*I)$_2$ crystals. Ag(*D*Cl)$_2$ and Ag(*D*Br)$_2$ gave quantitatively similar results of TG-DTA.

3.3. Photochemical control of electrical and magnetic properties

The UV irradiation effects in the temperature dependences of the electrical resistivity and the magnetic susceptibility of Ag(*D*I)$_2$ are shown in Figs. 5 and 6, respectively. The physical behavior of the pristine salt quantitatively agreed with previously reported one [32–43]. Ag(*D*I)$_2$ exhibited semiconducting behavior, i.e. thermally activated types of electrical and magnetic properties, at all the temperature range of measurements. After 72 h of UV irradiation, both of resistivity and activation energy clearly increased (Fig. 5). The increase in both of resistivity and activation energy can be interpreted that lattice defects should increase in the irradiated sample and that the unpaired electrons should decrease in number. The temperature and the irradiation-time dependences of the magnetic susceptibility (Fig. 6(a)) clearly showed that Ag(*D*I)$_2$, which exhibited a paramagnetic susceptibility at all the temperature of measurements,

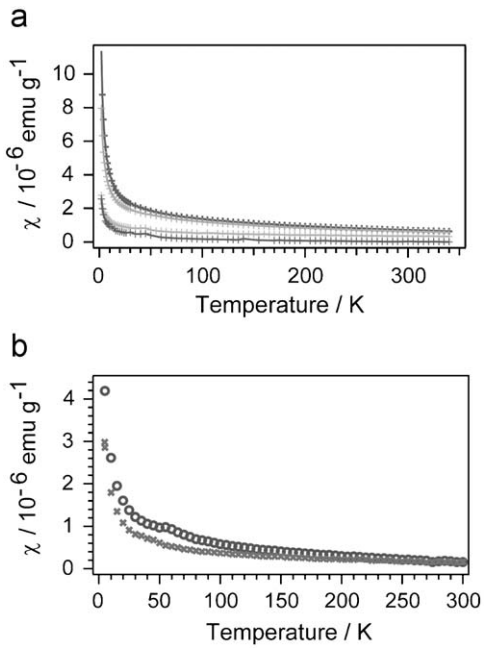

Fig. 6. UV irradiation effects in the magnetic susceptibility of Ag(*DI*)$_2$ measured on powder samples under continuous irradiation. Since the irradiated sample could be a mixture of Ag(*DI*)$_2$ and AgI, and the chemical composition could vary in accordance with irradiation, the susceptibility is shown as that per gram without subtraction of the core (diamagnetic) contribution. (a) Temperature-dependence of pristine (0 h) and irradiated for 6, 12 and 24 h with UV light (240–360 nm) in the order of the duration of irradiation from top to bottom. The sample temperature did not exceed 30 °C during irradiation. (b) Temperature-dependence of pristine (0 h; crosses) and irradiated for 3.5 h (circles) with UV–Vis light (220–1100 nm). The sample temperature was 45–50 °C during irradiation.

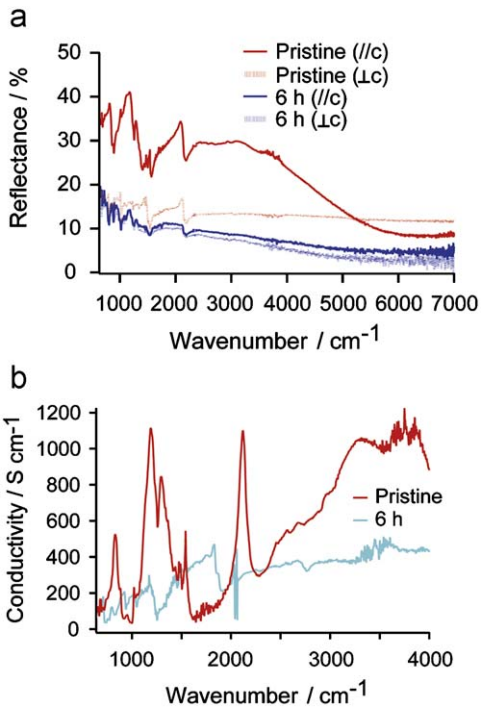

Fig. 7. Polarized (a) reflectance and (b) conductivity spectra measured on pristine and UV irradiated (6 h) single crystals of Ag(*DI*)$_2$. The polarization is (a) parallel or perpendicular, and (b) parallel to the *c* axis.

progressively turned into a diamagnetic material with UV irradiation. This indicates that the unpaired electrons in the sample should decrease in number in accordance with the irradiation. Interestingly, a similar irradiation with UV–Vis light (220–1100 nm) increased the paramagnetic susceptibility of Ag(*DI*)$_2$ (Fig. 6(b)). Since other conditions during the irradiation were identical with those of UV irradiation, the difference in irradiation effects on the paramagnetic susceptibility of Ag(*DI*)$_2$ was connected with one of the following two origins or both; (a) a wavelength-dependence of photochemical reaction(s) associated with this phenomenon, and (b) difference in heating effects associated with irradiation. In either case, wavelengths are important to control the magnetic susceptibility of Ag(*DI*)$_2$.

Reflectance spectra at IR region are shown in Fig. 7(a). As for the spectra of the pristine single crystal, a broad and intense band was observed at $\lesssim$6000 cm^{-1} when the polarization was parallel to the crystallographic *c* axis (||*c*-spectrum). This dispersion is associated with the conduction electrons. On the other hand such dispersion was not observed when the polarization was perpendicular to the *c* axis ($\perp$*c*-spectrum). This indicates that the conduction should occur only along the *c* axis, showing the one-dimensionality of the electronic structure of Ag(*DI*)$_2$ and being consistent with a previous optical study of this salt [43]. After UV irradiation for 6 h, the spectra became featureless irrespective of the polarization directions. The conductivity spectra (Fig. 7(b)), which were obtained by Kramers–Kronig transformation of the reflectance ||*c*-spectrum, also show evident decrease in oscillation strength in all through the IR region after irradiation for 6 h. This indicates that optical conductivity should significantly decrease after the UV irradiation. In short, the optical results support the interpretation that UV irradiation turned the paramagnetism into diamagnetism in Ag(*DI*)$_2$, and are consistent with the results

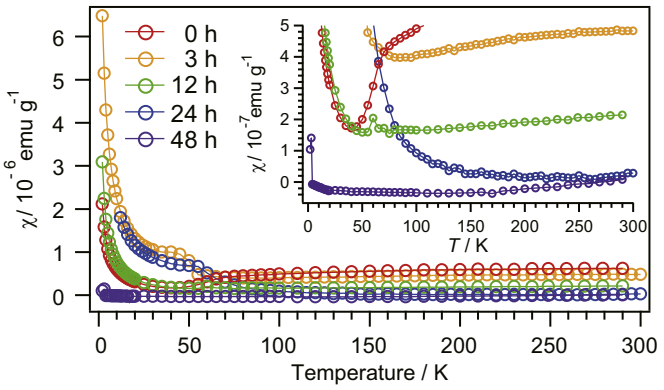

Fig. 8. UV irradiation effects in the magnetic susceptibility of Ag(*DCl*)$_2$ measured on powder samples under continuous irradiation; temperature-dependence of pristine (0 h) and irradiated for 3, 12, 24 and 48 h with UV light (240–360 nm). (inset: close-up view of increasing diamagnetic behavior of irradiated samples) Since the irradiated sample could be a mixture of Ag(*DCl*)$_2$ and AgCl, and the chemical composition could vary in accordance with irradiation, the susceptibility is shown as that per gram without subtraction of the core (diamagnetic) contribution. The sample temperature did not exceed 30 °C during irradiation.

of resistivity and magnetic susceptibility measurements mentioned above. One cannot quantitatively compare the results in Figs. 5–7, since the irradiation conditions were different among Figs. 5 and 7 (light source (A), single crystals) and Fig. 6 (light source (B), fine powder). However, all these results are consistent in that continuous UV irradiation turned paramagnetism into diamagnetism in Ag(*DI*)$_2$.

Similarly, the temperature dependences of the magnetic susceptibility of Ag(*DCl*)$_2$ are shown in Fig. 8. The behavior of the pristine salt quantitatively agreed with previously reported one [32–42]. Ag(*DCl*)$_2$ exhibited Pauli paramagnetism from RT down to ~70 K, at which a transition to a non-magnetic state was observed. This behavior is consistent with the reported metal-to-insulator

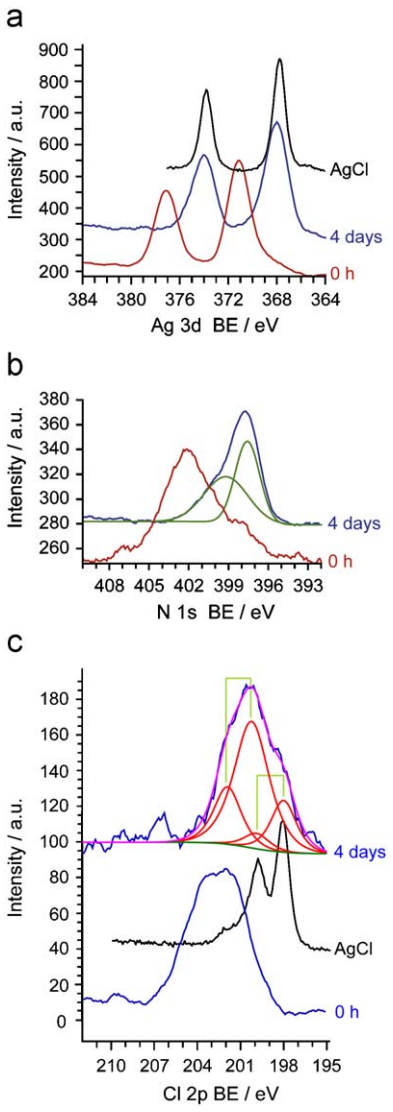

Fig. 9. XPS of pristine (0 h; red line) and irradiated (for 4 days) (4 days; blue line) Ag(*D*Cl)$_2$, and AgCl (authentic sample) (black line). (a) Ag 3*d*3/2 and 3*d*5/2, (b) N 1*s*, and (c) Cl 2*p*1/2 and 2*p*3/2 spectra. For the spectra of irradiated sample in (b), deconvoluted components are shown by green lines. For the spectra of irradiated sample in (c), deconvoluted components, their sum and assumed baseline are shown by red, purple and green lines, respectively. Each of the spin–orbit split doublets (2*p*1/2 and 2*p*3/2) is paired by pale green lines in (c). (For interpretation of the references to color in this figure legend, the reader is referred to the web version of this article.)

transition at ~70 K in Ag(*D*Cl)$_2$ [40]. On irradiation with UV light, the paramagnetic susceptibility began to decrease and finally the sample became non-magnetic in almost all the temperature range after irradiation for ~48 h. This fact indicates that the unpaired electrons, which are responsible for the electrical and magnetic properties, decreases in Ag(*D*Cl)$_2$. Such change in magnetic property was well reproducible; the absolute values and the temperature dependence of the paramagnetic susceptibility ($\geq$70 K) could be finely controlled by irradiation time. The electrical resistivity of the pristine and the irradiated Ag(*D*Cl)$_2$ single crystals could not be measured because their single crystals of sufficient dimensions were not obtained.

The Pauli-like paramagnetism of Ag(*D*Br)$_2$ also turned to diamagnetism after similar UV irradiation (not shown).

The XPS of the pristine and the irradiated (for four days) Ag(*D*Cl)$_2$ are shown in Figs. 9(a)–(c). As an authentic sample AgCl (99.5%, Wako) was also measured in the same condition and the spectra are shown in Figs. 9(a) and (c) as well. Because C 1*s* peaks in XPS often include signals due to impurities, the C 1*s* spectra are given in Fig. S3 (Supplementary material) and are not discussed here. The irradiated sample was confirmed to be ESR-silent, i.e. practically diamagnetic, at RT. Before irradiation, Ag 3*d*, N 1*s* and Cl 2*p* exhibited nearly symmetric peaks at 377.1 (Ag 3*d*3/2), 371.1 (Ag 3*d*5/2), 402.1 (N 1*s*) and ~202.5 eV (Cl 2*p*), respectively. In the unit cell of Ag(*D*Cl)$_2$, only one half of the *D*Cl molecule is crystallographically independent, containing four C, two N and one Cl atoms with different chemical environments from each other. Considering the energy resolution of XPS and π-conjugation in the *D*Cl molecule, the atoms of the same element should give a singly enveloped or poorly resolved peak in each XPS spectrum. XPS of organic charge transfer salts are previously discussed in detail [44], and thus spectral features concerning the pristine sample are not discussed here. After UV irradiation for four days, all the peaks shifted toward low BE. The resultant peak positions of Ag 3*d*5/2 and 3*d*3/2 almost agreed with those of AgCl. After deconvolution, one of the doublets in the Cl 2*p* spectrum also has close BEs with those of AgCl. These facts indicate that the irradiated sample includes AgCl. At the same time, the XPS of N 1*s* and Cl 2*p* indicate that the irradiated sample also includes chemical species having different electronic states from those in Ag(*D*Cl)$_2$ (starting material) or those in AgCl (resultant material). The results of deconvolution were dependent on samples and irradiation times except for those assigned to Ag(*D*Cl)$_2$ or AgCl. Considering the related data (shown later in Figs. 10–12), such uncharacterized chemical species should be of undetectable amount by bulk spectroscopic methods or SEM, and could be a transient state instead of a well-defined (meta)stable chemical species. For comparison, non-irradiated surface of the same sample was also examined by XPS, and was confirmed to give an identical spectra with those of the pristine Ag(*D*Cl)$_2$. The borderline of irradiated and non-irradiated parts was clear and sharp, judging from the contrasting spectra obtained from both sides of the borderline. Accordingly, the spatial resolution of such photochemical modification was as high as those observed for a related salt [15]. In order to check how deeply the irradiation effects could reach, the other side of the same sample (a pellet irradiated only at the center) was also examined by XPS at every half a day, and an identical result was obtained on the sample irradiated for four days: only the other side of irradiated part showed the abovementioned shifts of the peaks, while the other side of non-irradiated part showed no change in the XPS compared with those of the pristine sample. From this fact, the quantum yield is roughly estimated to be ~0.2%. In conclusion from XPS, a part of Ag(*D*Cl)$_2$ decomposed to AgCl by UV irradiation with retaining the non-irradiated part intact. Such photochemical modification was effective at bulk level. Yet the decomposition to AgCl was not complete even for a practically diamagnetic sample.

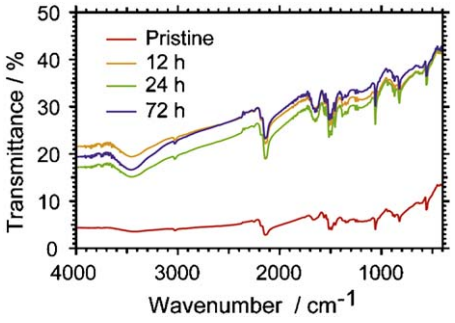

Fig. 10. IR spectra (KBr disk) of pristine and irradiated (for 12, 24 and 72 h) Ag(*D*Cl)$_2$. The same samples (except for 72 h) were used with those for magnetic susceptibility measurement (Fig. 8).

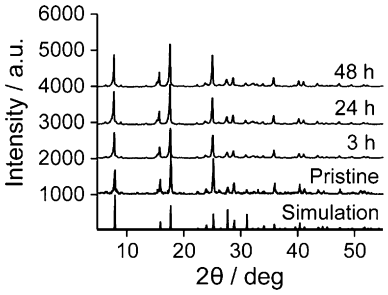

Fig. 11. Powder XRD patterns of pristine and irradiated (for 3, 24 and 48 h) Ag(*D*Cl)$_2$. Simulated pattern based on single crystal structural analysis is also shown for comparison. The same samples were used with those for magnetic susceptibility measurement (Fig. 8).

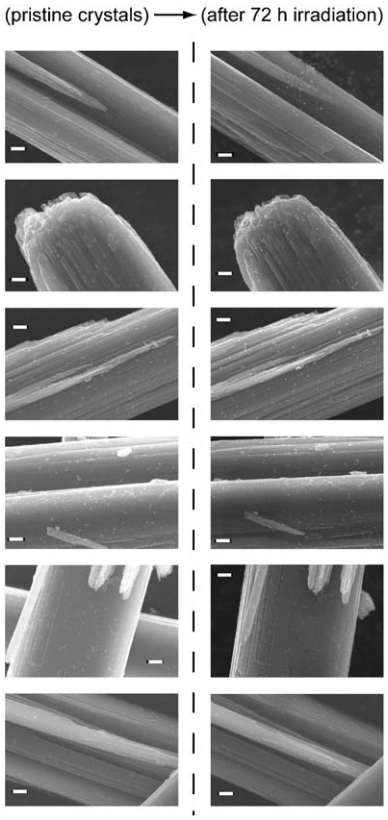

Fig. 12. Scanning electron microphotographs of arbitrarily selected surfaces of single crystals of Ag(*D*Cl)$_2$; before (left) and after (right) 72 h-UV-irradiation. All scale bars (white lines) indicate 1 μm.

This fact partly explains why the sample apparently kept its original shape in spite of the chemical decomposition. Because the physical properties of low-dimensional organic conductors are very sensitive to lattice defects, even a small amount of Ag*X* could effectively modify the electronic/magnetic properties of Ag(*DX*)$_2$ without making the original (crystalline) appearance collapse. More detailed structural analyses will clarify the exact amount of AgCl in Ag(*D*Cl)$_2$ in irradiated samples, which is now under way and will be reported in due course.

3.4. Mechanism of photochemical control of the physical properties of Ag(*DX*)$_2$

Based on the measurements, the temperature of the samples was always less than 50 °C during the UV irradiation

Table 2
Summary of mass spectra of neutral *D*Cl molecule, pristine (0 h) and irradiated (48 h) Ag(*D*Cl)$_2$.

Sample	Detection mode	Detected formula weight, assignment	
*D*Cl (neutral)	Negative	224, *D*Cl	
Ag(*D*Cl)$_2$ (0 h)	Negative	224, *D*Cl	557, Ag(*D*Cl)$_2$
	Positive	109, Ag	224, *D*Cl
Ag(*D*Cl)$_2$ (48 h)	Negative	224, *D*Cl	557, Ag(*D*Cl)$_2$
	Positive	109, Ag	224, *D*Cl

The same samples were used with those for magnetic susceptibility measurement (Fig. 8).

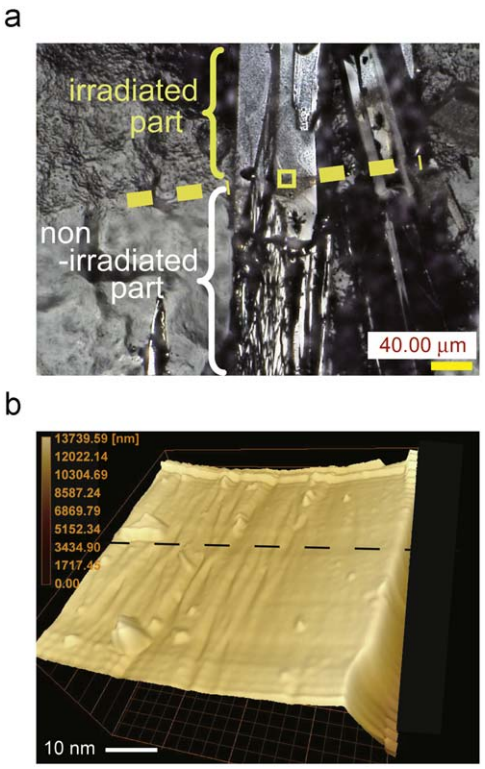

Fig. 13. Surface of crystalline Ag(*D*I)$_2$ irradiated for 3.5 h (light source (A)); (a) Digital microscope photograph, and (b) atomic force microscopy (AFM) 3D image (40 nm × 40 nm). The single crystal was irradiated with masked over a lower part as indicated in (a). AFM observation was carried out on the borderline of irradiated and non-irradiated parts as schematically indicated by yellow empty square in (a). The borderline is shown as a dotted line in (b). Observed roughness of the surface is depicted by darkness/brightness of the brown color in (b). (For interpretation of the references to color in this figure legend, the reader is referred to the web version of this article.)

irrespective of duration, light sources, and atmosphere of irradiation. The results of both DSC (including XRD–DSC) and TG-DTA indicated that Ag(*DX*)$_2$ should be thermochemically stable well below 170 °C irrespective of atmospheres and that decomposition of Ag(*DX*)$_2$ to Ag*X* began at ≥170 °C and continued up to ~370 °C. However, Ag*X* were detected in the irradiated Ag(*DX*)$_2$ with less paramagnetic or diamagnetic susceptibilities. This indicates that decomposition of Ag(*DX*)$_2$ to Ag*X* should progress during the UV irradiation mainly by photochemical reactions. A series of nearly identical spectra were obtained in IR (Fig. 10) and MS (Table 2) measurements for the samples irradiated for 0–72 h, which indicated that there were practically no impurities other than Ag*X* in the crystalline Ag(*DX*)$_2$ all through irradiation. The corresponding XRD patterns (Fig. 11) indicated that the original crystalline lattice of Ag(*DX*)$_2$ remained almost unchanged

immediately before it became totally diamagnetic (Fig. 8). The infinite coordination network between the Ag^+ cations and the NCN group of the *DM* radical anion species may be related to such robustness of the lattice of Ag(*DX*)$_2$, which could survive UV and/or heat only with partial decomposition, accommodate resultant Ag*X* and retain the crystalline state up to as high temperature as ~140 °C. We could not find any difference in the results of X-ray structural analysis of the single crystals of the pristine and the irradiated, diamagnetic Ag(*D*Cl)$_2$ by a laboratory equipment (Rigaku R-AXIS RAPID). Using SEM, no changes were observed in the appearances of the single crystals of Ag(*DX*)$_2$ after irradiation (Fig. 12), which excludes the possibility that UV irradiation caused damage to the samples accompanied by collapse of the original shapes such as melting, combustion, or sublimation. When a part of a single crystal of Ag(*DX*)$_2$ was irradiated with UV light, only the irradiated part was affected; the crystalline shape remained intact as a whole, but in the irradiated part the silvery color of the reflectance (indicating a highly conductive state) tinged with bluish tints (much less conductive) after irradiation, corresponding to the change in the electronic structure around the Fermi level and thus to the change in the physical properties (Fig. 13). This discussion is consistent with the IR reflectance spectra (Fig. 7), and would be further corroborated by reflectance spectra of UV–Vis region. There was a difference in height by 7 nm between highest and lowest points on the surface at the borderline of irradiated and non-irradiated parts (Fig. 13(b)), and averaged roughness of the surface shown in Fig. 13(b) was 1.0 nm. There were no traces on the surface such as islands of Ag*X* or holes left after loss of Ag(*DX*)$_2$. This means that the irradiated surface remained intact in a mechanical sense, being free of irradiation damage. All these results consistently show that the change in the physical properties of Ag(*DX*)$_2$ under UV irradiation is due to their decomposition to Ag*X* coexisting with the original lattice of Ag(*DX*)$_2$.

4. Conclusions

The irradiation with UV light on Ag(*DX*)$_2$ ($X = $ Cl, Br, I) altered their structural and physical properties with retaining the original macroscopic sample appearance (shape). This is due to decomposition of the crystalline, conductive and paramagnetic Ag(*DX*)$_2$ to insulating and diamagnetic Ag*X*. Only a partial decomposition is sufficient to make them practically diamagnetic at RT, and resultant Ag*X* is incorporated in the lattice of Ag(*DX*)$_2$. Ag(*DX*)$_2$ can be prepared as thin films on various substrates. Owing to the spatial resolution of the photochemical reactions, this irreversible and qualitative change could be utilized as optical writing and magnetic reading (write at once) in memory devices, since thin films of Ag(*DX*)$_2$ will irreversibly turn diamagnetic around RT by brief UV irradiation.

Acknowledgments

Elemental analyses were carried out at the Center for Instrumental Analysis, Hokkaido University. T.N. also thanks Dr. Shigeki Jin at the Open Facilities at Hokkaido University for their help with MALDI-TOF mass measurements. We thank Drs. Miho Sasaki and Akira Kishi (Rigaku Corporation) and Prof. Katsuaki Konishi (Hokkaido University) for their kind help in the thermal analyses and for valuable discussions. We thank Dr. Hiroyuki Mayama (Hokkaido University) for helping with the XRD measurements. We thank Profs. Shin-ichiro Noro, Tomoyuki Akutagawa and Takayoshi Nakamura (Hokkaido University) for their help in the SQUID measurements. This work is partially supported by the Hokkaido University Grant Program for Leading Edge Research, and also supported by the Grant-in-Aid for the Global COE Program "Catalysis as the Basis for Innovation in Materials Science" from the Ministry of Education, Culture, Sports, Science and Technology (MEXT) of Japan.

Appendix A. Supplementary material

Supplementary data associated with this article can be found in the online version at doi:10.1016/j.jssc.2009.07.032.

References

[1] H. Mori, J. Phys. Soc. Jpn. 75 (2006) 051003 15 pages.
[2] S. Kagoshima, K. Kanoda, T. Mori (Eds.), J. Phys. Soc. Jpn. 75 (2006).
[3] P. Batail (Guest Ed.), Molecular Conductors Thematic Issue, Chem. Rev. 104 (2004).
[4] M. Matsuda, T. Naito, T. Inabe, N. Hanasaki, H. Tajima, T. Otsuka, K. Awaga, B. Narymbetov, H. Kobayashi, J. Mater. Chem. 10 (2000) 631–636.
[5] N. Hanasaki, H. Tajima, M. Matsuda, T. Naito, T. Inabe, Phys. Rev. B 62 (2000) 5839–5842.
[6] M. Matsuda, T. Naito, T. Inabe, N. Hanasaki, H. Tajima, J. Mater. Chem. 11 (2001) 2493–2497.
[7] H. Tajima, N. Hanasaki, M. Matsuda, F. Sakai, T. Naito, T. Inabe, J. Solid State Chem. 168 (2002) 509–513.
[8] N. Hanasaki, M. Matsuda, H. Tajima, T. Naito, T. Inabe, J. Phys. Soc. Jpn. 72 (2003) 3226–3230.
[9] M. Matsuda, N. Hanasaki, H. Tajima, T. Naito, T. Inabe, J. Phys. Chem. Solids 65 (2004) 749–752.
[10] N. Hanasaki, M. Matsuda, H. Tajima, E. Ohmichi, T. Osada, T. Naito, T. Inabe, J. Phys. Soc. Jpn. 75 (2006) 033703 4 pages.
[11] H. Tajima, G. Yoshida, M. Matsuda, K. Nara, K. Kajita, Y. Nishio, N. Hanasaki, T. Naito, T. Inabe, Phys. Rev. B 78 (2008) 064424 8 pages.
[12] T. Miyamoto, H. Niimi, W.-J. Chun, Y. Kitajima, H. Sugawara, T. Inabe, T. Naito, K. Asakura, Chem. Lett. 36 (2007) 1008–1009.
[13] H. Kobayashi, R. Kato, A. Kobayashi, Y. Nishio, K. Kajita, W. Sasaki, Chem. Lett. 15 (1986) 789–792.
[14] R. Kato, H. Kobayashi, A. Kobayashi, S. Moriyama, Y. Nishio, K. Kajita, W. Sasaki, Chem. Lett. 16 (1987) 507–510.
[15] T. Naito, T. Inabe, H. Niimi, K. Asakura, Adv. Mater. 16 (2004) 1786–1790.
[16] T. Naito, H. Sugawara, T. Inabe, Y. Kitajima, T. Miyamoto, H. Niimi, K. Asakura, Adv. Func. Mater. 17 (2007) 1663–1670.
[17] T. Naito, H. Sugawara, T. Inabe, Nanotechnology 18 (2007) 424008 8 pages.
[18] T. Naito, H. Sugawara, T. Inabe, T. Miyamoto, H. Niimi, K. Asakura, J. Non-Cryst. Solids 352 (2006) 2628–2630.
[19] T. Naito, H. Sugawara, T. Inabe, Y. Kitajima, T. Miyamoto, H. Niimi, K. Asakura, J. Low Temp. Phys. 142 (2006) 383–386.
[20] T. Naito, H. Sugawara, T. Inabe, T. Miyamoto, H. Niimi, K. Asakura, Mol. Cryst. Liq. Cryst. 455 (2006) 311–316.
[21] T. Naito, H. Sugawara, T. Inabe, T. Miyamoto, H. Niimi, K. Asakura, in: G. Saito, F. Wudl, R.C. Haddon, K. Tanigaki, T. Enoki, H.E. Katz, M. Maesato, (Eds.), Multifunctional Conducting Molecular Materials, RSC Publishing, The Royal Society of Chemistry, Cambridge, UK, 2007, pp. 181–184.
[22] A. Aumüller, S. Hünig, Liebigs Ann. Chem. 1 (1986) 142–164.
[23] S. Hünig, M. Kemmer, H. Meixner, K. Sinzger, H. Werner, T. Bauer, E. Tillmanns, F.R. Lux, M. Hollstein, H.-G. Groβ, U. Langohr, H.-P. Werner, J.U. von Schütz, H.-C. Wolf, Eur. J. Inorg. Chem. 1999 (1999) 899–916.
[25] G.M. Sheldrick, Acta Cryst. A 64 (2008) 112–122.
[26] D.T. Cromer, J.T. Waber, in: International Tables for X-ray Crystallography, vol. IV, The Kynoch Press, Birmingham, England, 1974 (Table 2.2 A).
[27] D.C. Creagh, J.H. Hubbell, in: A.J.C. Wilson (Ed.), International Tables for Crystallography, vol. C, Kluwer Academic Publishers, Boston, 1992, pp. 200–206 (Table 4.2.4.3).
[28] CrystalStructure 3.8: Crystal Structure Analysis Package, Rigaku and Rigaku/MSC, 9009 New Trails Dr., The Woodlands, TX 77381, USA, 2000–2006.
[30] L.J. Farrugia, J. Appl. Crystallogr. 30 (1997) 565 the program is available from the following URL, http://www.chem.gla.ac.uk/~louis/software/ortep3/.
[31] Kagaku Binran Kiso-Hen II, The Chemical Society of Japan, third ed., Maruzen, Tokyo, 1984, p. 509 (in Japanese).
[32] K. Hiraki, K. Kanoda, Phys. Rev. B 54 (1996) R17276–R17279.
[33] K. Hiraki, K. Kanoda, Synth. Met. 86 (1997) 2103–2104.
[34] K. Hiraki, K. Kanoda, Phys. Rev. Lett. 80 (1998) 4737–4740.
[35] K. Hiraki, K. Kanoda, Synth. Met. 103 (1999) 2090–2091.
[36] Y. Haruyama, K.G. Nath, S. Kimura, Y. Ufuktepe, T. Kinoshita, K. Hiraki, K. Kanoda, Solid State Commun. 110 (1999) 17–22.
[37] Y. Nogami, K. Oshima, K. Hiraki, K. Kanoda, J. Phys. IV 9 (1999) 357–359.

[38] T. Sakurai, N. Nakagawa, S. Okubo, H. Ohta, K. Kanoda, K. Hiraki, J. Phys. Soc. Jpn. 70 (2001) 1794–1800.
[39] T. Itou, K. Hiraki, H. Taniguchi, K. Kanoda, T. Takahashi, Phys. Rev. Lett. 89 (2002) 246402 4 pages.
[40] K. Hiraki, S. Suzuki, T. Takahashi, Synth. Met. 133–134 (2003) 419–420.
[41] T. Kakiuchi, Y. Wakabayashi, H. Sawa, T. Itou, K. Kanoda, Phys. Rev. Lett. 98 (2007) 066402 4 pages.
[42] S. Hünig, A. Aumüller, P. Erk, H. Meixner, J.U. von Schütz, H.-J. Gross, U. Langohr, H.-P. Werner, H.C. Wolf, Ch. Burschka, G. Klebe, K. Peters, H.G.v. Schnering, Synth. Met. 27 (1988) 181–188.
[43] K. Yamamoto, T. Yamamoto, K. Yakushi, C. Pecile, M. Meneghetti, Phys. Rev. B 71 (2005) 045118 10 pages.
[44] M. Sing, U. Schwingenschlogl, R. Claessen, M. Dressel, C.S. Jacobsen, cond-mat/0208422v3, 2003.